

Binwise exploration of vector couplings in $B_s \rightarrow D_s^{(*)}\tau\bar{\nu}_\tau$ decays

Ajay Kumar Yadav* and Suchismita Sahoo†

Department of Physics, Central University of Karnataka, Kalaburagi-585367, India

Abstract

Recent results from the LHCb experiment have confirmed that lepton flavor universality is upheld in flavor-changing neutral current processes, such as $B \rightarrow K^{(*)}l^+l^-$. However, discrepancies remain in the charged current sector, raising questions about the universality of lepton flavors in these processes. To explore this issue, we investigate the decays $B_s \rightarrow D_s^{(*)}\tau\bar{\nu}_\tau$ in different q^2 bins, which involve the $b \rightarrow c\tau\bar{\nu}_\tau$ transition. We employ a model-independent approach to analyze potential new physics by fitting both real and complex (axial)vector coefficients to the existing $b \rightarrow (u,c)\tau\bar{\nu}_\tau$ data. Our analysis enables us to calculate the branching ratios and angular distributions for the $B_s \rightarrow D_s^{(*)}\tau\bar{\nu}_\tau$ decays in four different q^2 bins. Additionally, we evaluate whether lepton flavor universality is maintained in these charged current decays or if deviations suggest the presence of new physics.

*Electronic address: yadavajaykumar286@gmail.com

†Electronic address: suchismita8792@gmail.com

I. INTRODUCTION

The Standard Model (SM) is successful in many predictions but falls short in explaining matter-antimatter asymmetry, neutrino mass, dark matter, dark energy, and other anomalies. Recent deviations in semileptonic B meson decays from the SM expectations suggest potential new physics (NP), as observed in measurements of $R_{D^{(*)}}$, $R_{J/\Psi}$, and the τ polarization asymmetry [1–7]. Experimentally, the BaBar [8, 9], Belle [10–12], and LHCb [13, 14] collaborations have measured the ratios of branching fractions as

$$R_{D^{(*)}} = \frac{BR(B \rightarrow D^{(*)}\tau\bar{\nu}_\tau)}{BR(B \rightarrow D^{(*)}l\bar{\nu}_l)}, \quad R_{J/\Psi} = \frac{BR(B_c \rightarrow J/\Psi\tau\bar{\nu}_\tau)}{BR(B_c \rightarrow J/\Psi l\bar{\nu}_l)}, \quad \text{where } l = e, \mu. \quad (1)$$

The Heavy Flavor Averaging Group (HFLAV) reports the average values [15]

$$R_D^{\text{avg}} = 0.357 \pm 0.029, \quad R_{D^{(*)}}^{\text{avg}} = 0.284 \pm 0.012, \quad (2)$$

which exceed the SM predictions [16, 17]

$$R_D^{\text{SM}} = 0.299 \pm 0.011, \quad R_{D^{(*)}}^{\text{SM}} = 0.252 \pm 0.003, \quad (3)$$

by 2.16σ and 2.26σ respectively. Likewise, the ratio $R_{J/\Psi}$ measured by the LHCb[18] experiment

$$R_{J/\Psi} = 0.71 \pm 0.17 \pm 0.18 \quad R_{J/\Psi}^{\text{SM}} = 0.289 \pm 0.01, \quad (4)$$

shows a disagreement of 1.8σ [19] from the SM prediction at the 95% confidence level. This discrepancy suggests a potential violation of lepton flavor universality (LFU) between the tau lepton and the lighter leptons. Semileptonic B decays involving $b \rightarrow c\tau\bar{\nu}_\tau$ flavor-changing charged currents (FCCC) are key for testing SM predictions, exploring potential lepton flavor universality violations (LFUV) and investigating NP beyond the SM.

This study aims to perform a binwise analysis of the decay processes $B_s \rightarrow D_s^{(*)}\tau\bar{\nu}_\tau$, which include the $b \rightarrow c\tau\bar{\nu}_\tau$ quark-level transition, in a model-independent approach by extending the operator structure of the Lagrangian beyond the SM. In this formalism, we identify additional (axial)vector Wilson coefficients that contribute to the SM coefficients. By performing a χ^2 fit to $b \rightarrow (u, c)\tau\bar{\nu}_\tau$ data, we determine the best-fit values for these new real and complex parameters. We estimate the binwise branching ratios, forward-backward asymmetries, lepton non-universality (LNU) ratios, and the polarization asymmetries of τ and D_s^* for $B_s \rightarrow D_s^{(*)}\tau\bar{\nu}_\tau$ decay modes with both real and complex new coefficients. The

theoretical analysis of these decay modes, both in model-dependent and model-independent frameworks, can be found in the literature [20–31].

The paper is organized as follows. Section II presents the effective Hamiltonian for semileptonic decays involving the quark level transition $b \rightarrow c\tau\bar{\nu}_\tau$ and details the global fit of both real and complex (axial)vector Wilson coefficients using $b \rightarrow (u, c)\tau\bar{\nu}_\tau$ experimental data. Section III provides detailed expressions for the branching ratios and various angular observables of $B_s \rightarrow D_s^{(*)}\tau\bar{\nu}_\tau$ decays and includes the numerical evaluation of $B_s \rightarrow D_s^{(*)}\tau\bar{\nu}_\tau$ decay modes with the constrained new parameters. Finally, Section IV summarizes our results.

II. THEORETICAL MODEL FORMULATION

A. Effective Hamiltonian

The effective Hamiltonian responsible for the $b \rightarrow c\tau\bar{\nu}_\tau$ transitions, including only the (axial)vector operator structure extension, is given by [32]

$$\mathcal{H}_{\text{eff}} = \frac{4G_F}{\sqrt{2}} V_{cb} [(1 + V_L) \mathcal{O}_{V_L} + V_R \mathcal{O}_{V_R}], \quad (5)$$

where G_F is the Fermi constant, V_{cb} is the CKM matrix element, and $V_{L,R}$ are the Wilson coefficients, which are zero in the SM and can arise only in the presence of new physics. The corresponding dimension-six effective operators ($\mathcal{O}_{V_{L,R}}$) are given by

$$\mathcal{O}_{V_L} = (\bar{c}_L \gamma^\mu b_L) (\bar{\tau}_L \gamma_\mu \nu_{lL}), \quad \mathcal{O}_{V_R} = (\bar{c}_R \gamma^\mu b_R) (\bar{\tau}_L \gamma_\mu \nu_{lL}),$$

where $f_{L(R)} = P_{L(R)} f$ are the chiral fermion f fields with $P_{L(R)} = (1 \mp \gamma_5)/2$ being the projection operators.

B. Numerical Fitting of Model Parameters

Assuming that the couplings for $b \rightarrow u$ and $b \rightarrow c$ transitions are identical, we perform a global fit of the new coefficients to the $b \rightarrow (u, c)\tau\bar{\nu}_\tau$ data. The χ^2 function is defined as

$$\chi^2(V_{L,R}) = \sum_i \frac{(\mathcal{O}_i^{\text{th}}(V_{L,R}) - \mathcal{O}_i^{\text{Expt}})^2}{(\Delta \mathcal{O}_i^{\text{Expt}})^2 + (\Delta \mathcal{O}_i^{\text{SM}})^2}, \quad (6)$$

where $\mathcal{O}_i^{\text{th}}(V_{L,R})$ denotes the theoretical predictions of the observables, $\mathcal{O}_i^{\text{Expt}}$ represents the corresponding experimental central values, and $\Delta\mathcal{O}_i^{\text{Expt}}$ and $\Delta\mathcal{O}_i^{\text{SM}}$ are the experimental and SM uncertainties, respectively. To scrutinize the signature of new (axial)vector coefficients, we analyzed several possible combinations of both real and complex Wilson coefficients. The details are provided in Table I.

1D Scenario		2D Scenario		4D Scenario	
Scenario	Coefficient	Scenario	Coefficient	Scenario	Coefficient
1DS-I	$Re[V_L]$	2DS-I	$(Re[V_L], Re[V_R])$	4DS-I	$(Re[V_L], Im[V_L], Re[V_R], Im[V_R])$
1DS-II	$Re[V_R]$	2DS-II	$(Re[V_L], Im[V_L])$		
		2DS-III	$(Re[V_R], Im[V_R])$		

TABLE I: Scenarios of new real and complex (axial)vector coefficients.

We explored six possible scenarios: two one-dimensional scenarios (1DS-I and 1DS-II), three two-dimensional scenarios (2DS-I, 2DS-II, and 2DS-III), and one four-dimensional scenario (4DS-I), fitting them to the observables of $b \rightarrow c\tau\bar{\nu}_\tau$ and $b \rightarrow u\tau\bar{\nu}_\tau$ in two different ways:

- Case **A**: Using only the observables associated with the $b \rightarrow c\tau\bar{\nu}_\tau$ data.
- Case **B**: Incorporating both $b \rightarrow c\tau\bar{\nu}_\tau$ and $b \rightarrow u\tau\bar{\nu}_\tau$ observables.

For the $b \rightarrow c\tau\bar{\nu}_\tau$ observables, we utilized existing data on $R_{D^{(*)}}$, $R_{J/\psi}$, $P_\tau^{D^*}$, $F_L^{D^*}$, and the branching ratio for $B_c \rightarrow \tau\bar{\nu}_\tau$, which is estimated to be less than 30% based on the lifetime of the B_c meson. Additionally, we fitted the observables R_π , $\text{BR}(B_u \rightarrow \tau\bar{\nu}_\tau)$, and $\text{BR}(B^0 \rightarrow \pi^+\tau\bar{\nu}_\tau)$ related to the $b \rightarrow u\tau\bar{\nu}_\tau$ transition using the new parameters. Details of these observables can be found in Table II.

After performing the global fit analysis for both Case **A** and Case **B**, we report the best-fit values along with their pull, defined as $\sqrt{\chi_{\text{SM}}^2 - \chi_{\text{best-fit}}^2}$, and the p-values (in %) presented in Table III. The contour plots of the new parameters associated with all the new scenarios for Case **A** and Case **B** are shown in Fig. 1 and 2, respectively. We observed that the percentage of the p-value has increased for the combined fit of the $b \rightarrow (u, c)\tau\bar{\nu}_\tau$ observables to the new parameters. The possible combinations of 2D coefficients yield the best p-values,

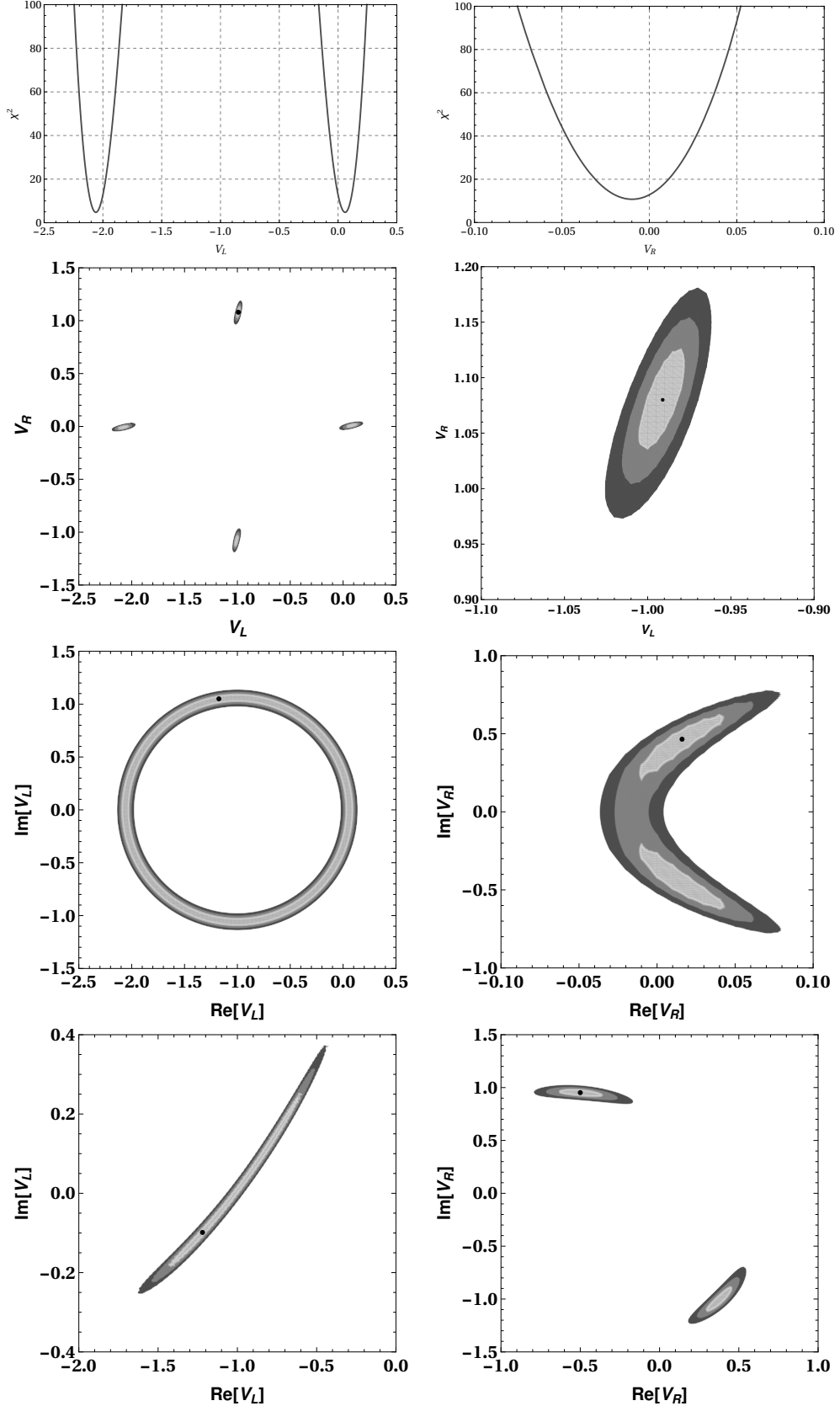


FIG. 1: χ^2 analysis plots for new physics scenarios in Case A, including axial(vector) coefficients, depicting the fit quality and confidence regions.

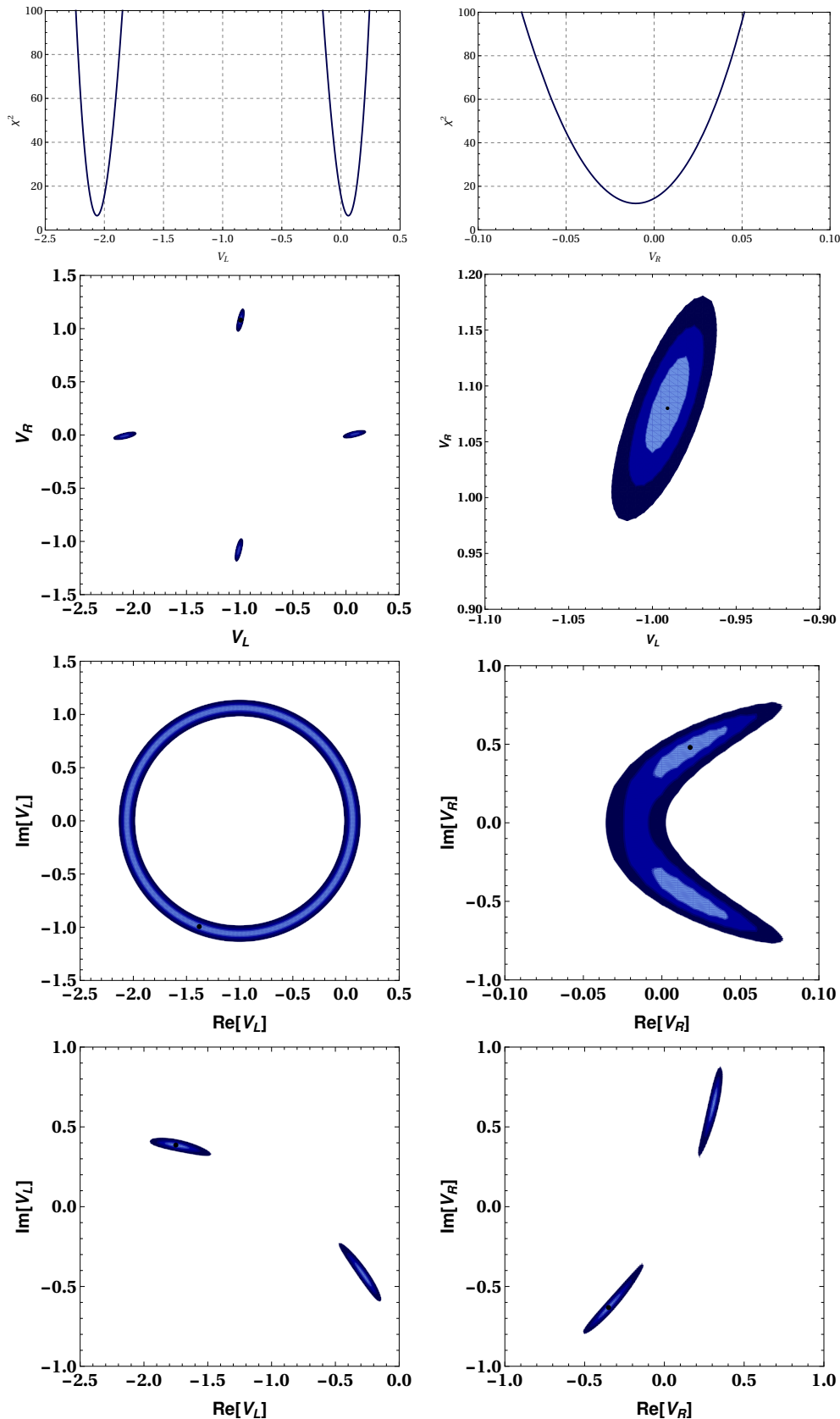


FIG. 2: Same as Fig. 1 for the Case B.

Observables	Experimental values	SM Predictions
R_D	0.342 ± 0.026	0.298 ± 0.004
R_{D^*}	0.287 ± 0.012	0.254 ± 0.005
$R_{J/\psi}$	$0.71 \pm 0.17 \pm 0.18$	0.289 ± 0.01
$P_\tau^{D^*}$	$-0.38^{+0.53}_{-0.55}$	-0.497 ± 0.007
$F_L^{D^*}$	0.60 ± 0.09	0.464 ± 0.003
$\text{Br}(B_c \rightarrow \tau \bar{\nu}_\tau)$	$< 30\%$	$(3.6 \pm 0.14) \times 10^{-2}$
R_π^l	0.699 ± 0.156	0.583 ± 0.055
$\text{BR}(B_u \rightarrow \tau \bar{\nu}_\tau)$	$(1.09 \pm 0.24) \times 10^{-4}$	$(8.48 \pm 0.5) \times 10^{-5}$
$\text{BR}(B^0 \rightarrow \pi^+ \tau \bar{\nu}_\tau)$	$< 2.5 \times 10^{-4}$	$(9.40 \pm 0.75) \times 10^{-5}$

TABLE II: Observed and theoretical values of quantities employed in the fitting process.

indicating the best fit to the experimental data. Thus, we are going to present the impact of these new physics scenarios of (axial)vector Wilson coefficients on the $B_s \rightarrow D_s^{(*)} \tau \bar{\nu}_\tau$ decay modes for Case **B**.

III. $B_s \rightarrow D_s^{(*)} \tau \bar{\nu}_\tau$ DECAY MODES

A. Mathematical Expressions for Key Observables

The branching ratio of the $\bar{B}_s \rightarrow D_s \tau \bar{\nu}_\tau$ process as a function of q^2 in the presence of new (axial)vector coefficients is given by [33]

$$\begin{aligned} \frac{d\text{BR}(\bar{B}_s \rightarrow D_s \tau \bar{\nu}_\tau)}{dq^2} = & \tau_B \frac{G_F^2 |V_{cb}|^2}{192\pi^3 M_B^3} q^2 \sqrt{\lambda_{D_s}(q^2)} \left(1 - \frac{m_\tau^2}{q^2}\right)^2 \\ & \times \left|1 + V_L + V_R\right|^2 \left[\left(1 + \frac{m_\tau^2}{2q^2}\right) H_0^2 + \frac{3}{2} \frac{m_\tau^2}{q^2} H_t^2 \right], \end{aligned} \quad (7)$$

where $\lambda_{D_s} = \lambda(M_B^2, M_{D_s}^2, q^2)$, with $\lambda(a, b, c) = a^2 + b^2 + c^2 - 2(ab + bc + ca)$ and $H_{0,t}$'s are the heicity amplitudes given in the appendix A.

Scenario	Coefficient	Best-fit value	Pull	p-value (%)
Case A				
1DS - I	$Re[V_L]$	-2.06	2.83	44.36
1DS - II	$Re[V_R]$	-0.01	1.44	5.67
2DS - I	$(Re[V_L], Re[V_R])$	(-0.991, 1.08)	2.99	40.96
2DS - II	$(Re[V_L], Im[V_L])$	(-1.175, 1.05)	2.83	31.09
2DS - III	$(Re[V_R], Im[V_R])$	(0.016, 0.465)	2.97	40.66
4DS - I	$(Re[V_L], Im[V_L], Re[V_R], Im[V_R])$	(-1.22, -0.099, -0.502, 0.952)	2.97	13.56
Case B				
1DS - I	$Re[V_L]$	-2.06	3.01	58.66
1DS - II	$Re[V_R]$	-0.01	1.52	14.61
2DS - I	$(Re[V_L], Re[V_R])$	(-0.99, 1.084)	3.18	73.14
2DS - II	$(Re[V_L], Im[V_L])$	(-1.38, -0.994)	3.014	62.02
2DS - III	$(Re[V_R], Im[V_R])$	(0.018, 0.475)	3.18	74.32
4DS - I	$(Re[V_L], Im[V_L], Re[V_R], Im[V_R])$	(-1.75, 0.39, -0.35, -0.632)	3.18	50.55

TABLE III: Best-fit, pull and p-value(%) of various new physics scenarios.

The branching ratios of $\bar{B} \rightarrow D_s^* \tau \bar{\nu}_\tau$ with respect to q^2 is given by [33]

$$\frac{d\text{BR}(\bar{B}_s \rightarrow D_s^* \tau \bar{\nu}_\tau)}{dq^2} = \tau_B \frac{G_F^2 |V_{cb}|^2}{192\pi^3 M_B^3} q^2 \sqrt{\lambda_{D_s^*}(q^2)} \left(1 - \frac{m_\tau^2}{q^2}\right)^2 \times \\ \left\{ (|1 + V_L|^2 + |V_R|^2) \left[\left(1 + \frac{m_\tau^2}{2q^2}\right) (H_{V,+}^2 + H_{V,-}^2 + H_{V,0}^2) + \frac{3}{2} \frac{m_\tau^2}{q^2} H_{V,t}^2 \right] \right. \\ \left. - 2\text{Re}[(1 + V_L) V_R^*] \left[\left(1 + \frac{m_\tau^2}{2q^2}\right) (H_{V,0}^2 + 2H_{V,+}H_{V,-}) + \frac{3}{2} \frac{m_\tau^2}{q^2} H_{V,t}^2 \right] \right\}, \quad (8)$$

where $\lambda_{D_s^*} = \lambda(M_B^2, M_{D_s^*}^2, q^2)$ and $H_{V,\lambda}$'s ($\lambda = +, -, 0$) are the helicity amplitudes presented in appendix A.

In addition to the branching ratios, we also examine the following observables [33] to investigate the structure of new physics.

- Lepton non-universality:

$$R_{D_s^{(*)}} = \frac{\text{BR}(B_s \rightarrow D_s^{(*)} \tau \bar{\nu}_\tau)}{\text{BR}(B_s \rightarrow D_s^{(*)} l \bar{\nu}_l)}, \quad l = e, \mu. \quad (9)$$

- τ forward-backward asymmetry:

$$A_{\text{FB}}^{D_s^{(*)}} = \frac{\int_0^1 \frac{d\Gamma}{d\cos\theta} d\cos\theta - \int_{-1}^0 \frac{d\Gamma}{d\cos\theta} d\cos\theta}{\int_{-1}^1 \frac{d\Gamma}{d\cos\theta} d\cos\theta}. \quad (10)$$

- τ forward and backward fractions:

$$\chi_{1,2}^{D_s^{(*)}} = \frac{1}{2} R_{D_s^{(*)}} \left(1 \pm A_{FB}^{D_s^{(*)}} \right). \quad (11)$$

- τ polarization asymmetry:

$$P_\tau^{D_s^{(*)}}(q^2) = \frac{d\Gamma(\lambda_\tau = 1/2)/dq^2 - d\Gamma(\lambda_\tau = -1/2)/dq^2}{d\Gamma(\lambda_\tau = 1/2)/dq^2 + d\Gamma(\lambda_\tau = -1/2)/dq^2}. \quad (12)$$

- τ spin 1/2 and -1/2 fractions:

$$\chi_{3,4}^{D_s^{(*)}} = \frac{1}{2} R_{D_s^{(*)}} \left(1 \pm P_\tau^{D_s^{(*)}} \right). \quad (13)$$

- D_s^* polarization asymmetry:

$$F_{L,T}^{D_s^*}(q^2) = \frac{d\Gamma_{L,T}(B_s \rightarrow D_s^* \tau \bar{\nu})/dq^2}{d\Gamma(B_s \rightarrow D_s^* \tau \bar{\nu})/dq^2}. \quad (14)$$

- D_s^* longitudinal and transverse polarization fractions:

$$\chi_{5,6}^{D_s^*} = R_{D_s^*} F_{L,T}^{D_s^*}. \quad (15)$$

B. Results and Discussion

After collecting all the expressions for the branching ratios and key observables of the $B_s \rightarrow D_s^{(*)} \tau \bar{\nu}_\tau$ decay modes, we now proceed with the numerical analysis. For this analysis, we have taken the necessary input parameters from the PDG [34] and the form factors for both $B_s \rightarrow D_s$ and $B_s \rightarrow D_s^*$ computed using the Lattice QCD method from [35] and [36], respectively. Using the best-fit values from all the new physics scenarios (1D, 2D, and 4D), we computed the branching ratios, lepton non-universality, forward-backward asymmetry, and $\chi_{1,\dots,6}^{D_s^{(*)}}$ observables in four different q^2 bins: $q^2 \in [3.2, 5] \text{ GeV}^2$, $q^2 \in [5, 7] \text{ GeV}^2$, $q^2 \in [7, 9] \text{ GeV}^2$, and $q^2 \in [9, q_{\max}^2] \text{ GeV}^2$. The left (right) panel of Fig. 3 depicts the branching ratio $\text{BR}(B_s \rightarrow D_s^{(*)} \tau \bar{\nu}_\tau)$ in all the new physics scenarios. The lepton non-universality parameters R_{D_s} (left panel) and $R_{D_s^*}$ (right panel) are shown in Fig. 4. The q^2 binwise

predictions for the forward-backward asymmetries, $A_{FB}^{D_s}$ (top left panel) and $A_{FB}^{D_s^*}$ (top right panel), as well as the observables $\chi_{1,2}^{D_s}$ (left panel) and $\chi_{1,2}^{D_s^*}$ (right panel) are presented in the middle and bottom panels of Fig. 5, respectively. Fig. 6 represents similar results as Fig. 5 for the τ polarization asymmetries $P_\tau^{D_s^{(*)}}$ and the observables $\chi_{3,4}^{D_s^*}$. The longitudinal (transverse) polarization asymmetry of D_s^* is presented in the top left (top right) panel of Fig. 7, while the bottom left (bottom right) panel represents the observables $\chi_{5,6}^{D_s^*}$. Here, the

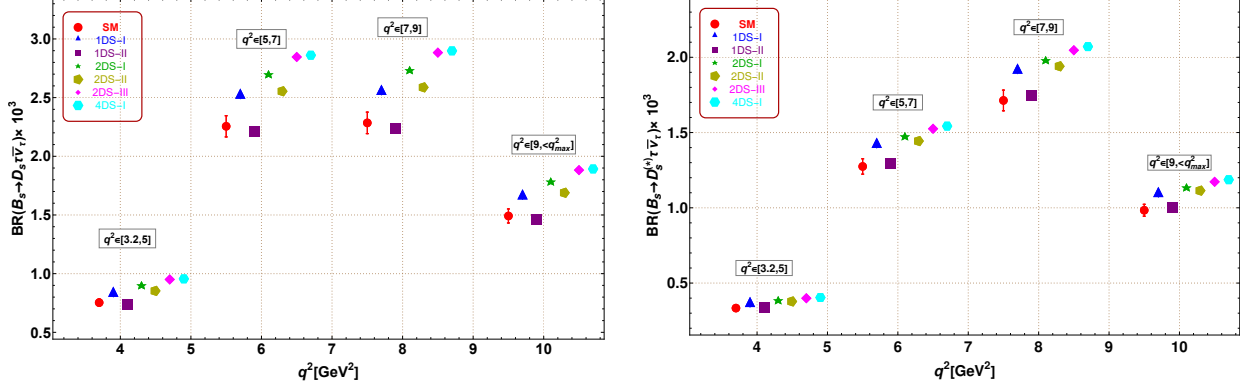


FIG. 3: The q^2 binwise predictions for the branching ratios of $B_s \rightarrow D_s \tau \bar{\nu}_\tau$ (left panel) and $B_s \rightarrow D_s^* \tau \bar{\nu}_\tau$ (right panel) decay processes are shown for all new physics scenarios. The red circle represents the SM central value prediction, and the red error lines indicate the 1σ theoretical uncertainties. Predictions from the various new physics scenarios are presented in different colors.

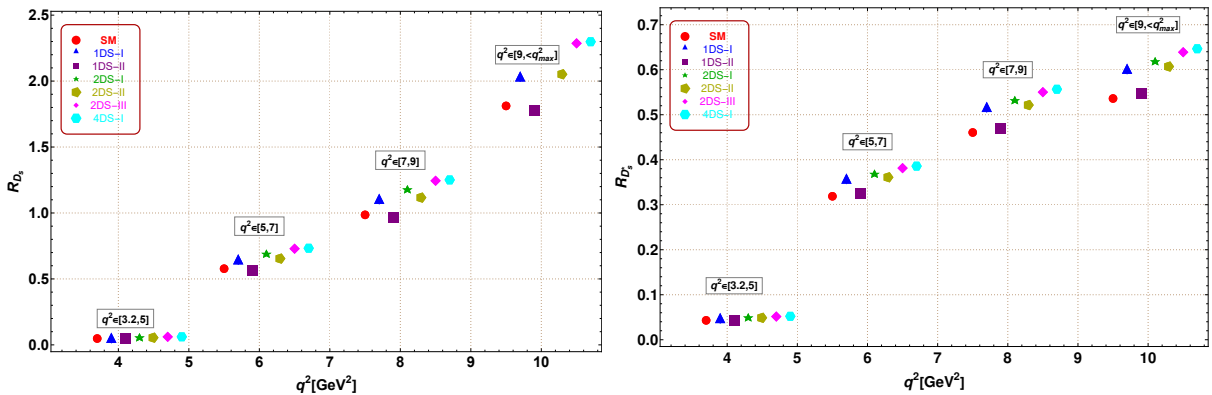


FIG. 4: Same as Fig. 3 for R_{D_s} (left panel) and $R_{D_s^*}$ (right panel).

red circle (error line) represents the central values of the Standard Model (SM) along with the 1σ theoretical uncertainties. The predictions from the best-fit values of all the scenarios are presented in different graphics and colors: 1DS-I \rightarrow Blue, 2DS-I \rightarrow Purple, 2DS-II \rightarrow

Green, 2DS-III → Dark Yellow, 2DS-IV → Magenta, and 4DS-I → Cyan. The numerical values of the branching ratios and other physical observables for the decay $B_s \rightarrow D_s \tau \bar{\nu}_\tau$ in the SM and all the new physics scenarios across the four different q^2 bins are presented in Table IV. Tables V and VI include the numerical values of the observables for the process $B_s \rightarrow D_s^* \tau \bar{\nu}_\tau$.

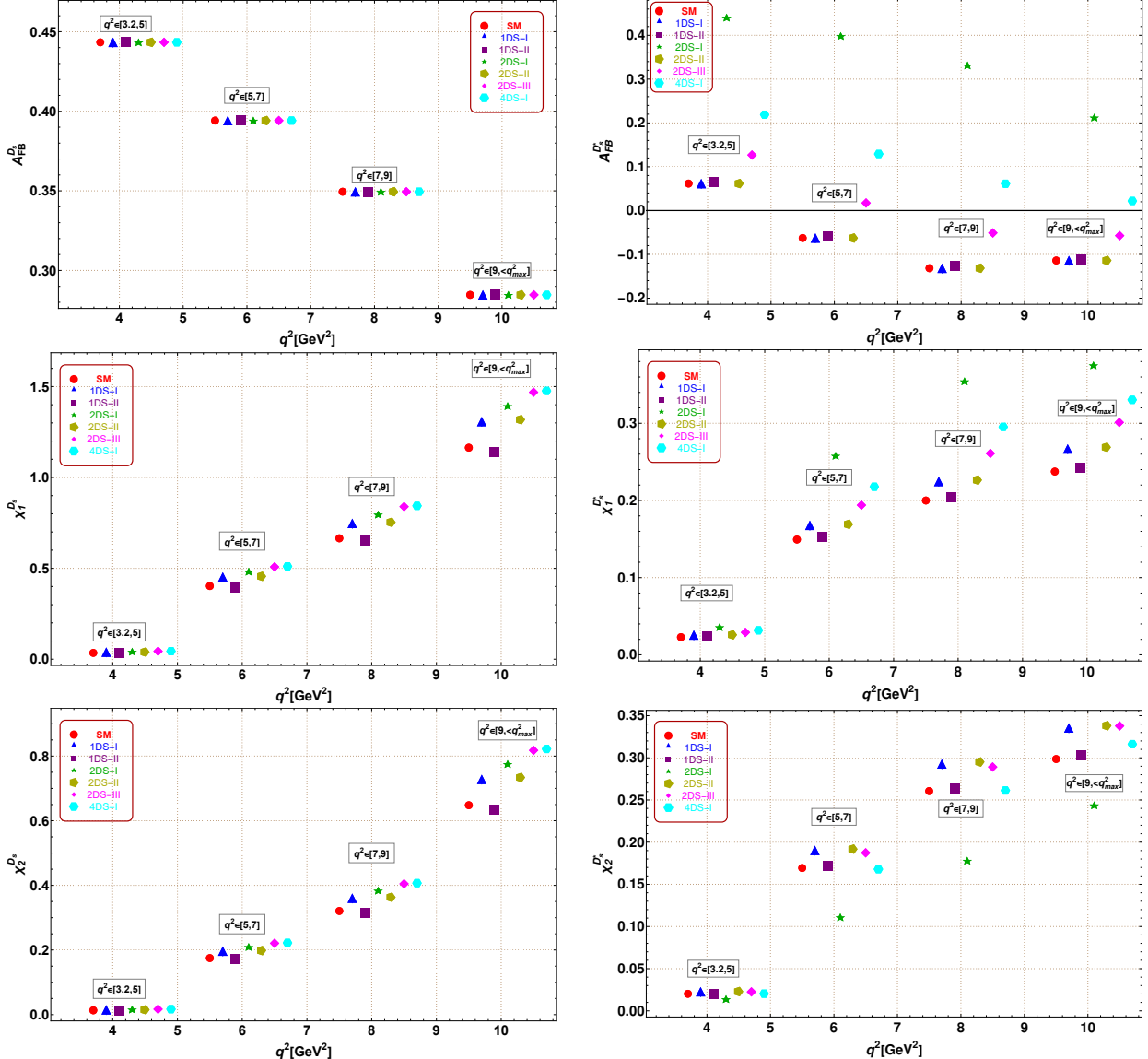


FIG. 5: Same as Fig. 3 for $A_{FB}^{D_s}$ (top left panel), $A_{FB}^{D^*}$ (top right panel), $\chi_1^{D_s}$ (middle left panel), $\chi_1^{D^*}$ (middle right panel), $\chi_2^{D_s}$ (bottom left panel) and $\chi_2^{D^*}$ (bottom right panel).

By analyzing the physical observables in the SM and in the presence of various new physics scenarios, we observed the following:

Scenarios	$BR \times 10^3$	R_{D_s}	$A_{FB}^{D_s}$	$P_\tau^{D_s}$	$\chi_1^{D_s}$	$\chi_2^{D_s}$	$\chi_3^{D_s}$	$\chi_4^{D_s}$
$q^2 \in [3.2 - 5] \text{ GeV}^2$								
SM	0.753	0.048	0.443	0.31	0.035	0.013	0.032	0.017
1DS-I	0.846	0.054	0.443	0.31	0.039	0.015	0.035	0.019
1DS-II	0.738	0.047	0.443	0.31	0.034	0.013	0.031	0.016
2DS-I	0.901	0.058	0.443	0.31	0.042	0.016	0.038	0.02
2DS-II	0.853	0.054	0.443	0.31	0.039	0.015	0.036	0.019
2DS-III	0.951	0.061	0.443	0.31	0.044	0.017	0.04	0.021
4DS-I	0.956	0.061	0.443	0.31	0.044	0.017	0.04	0.021
$q^2 \in [5 - 7] \text{ GeV}^2$								
SM	2.255	0.578	0.394	0.251	0.403	0.175	0.361	0.216
1DS-I	2.534	0.65	0.394	0.251	0.452	0.197	0.406	0.243
1DS-II	2.211	0.566	0.394	0.251	0.395	0.171	0.354	0.212
2DS-I	2.699	0.691	0.394	0.251	0.482	0.209	0.294	0.259
2DS-II	2.554	0.654	0.394	0.251	0.456	0.198	2.124	0.245
2DS-III	2.846	0.729	0.394	0.251	0.508	0.221	0.1	0.273
4DS-I	2.861	0.733	0.394	0.251	0.511	0.222	0.462	0.275
$q^2 \in [7 - 9] \text{ GeV}^2$								
SM	2.285	0.986	0.349	0.277	0.665	0.321	0.63	0.357
1DS-I	2.567	1.108	0.349	0.277	0.747	0.360	0.707	0.401
1DS-II	2.239	0.966	0.349	0.277	0.652	0.314	0.617	0.349
2DS-I	2.734	1.180	0.349	0.277	0.796	0.384	0.753	0.427
2DS-II	2.587	1.116	0.349	0.277	0.753	0.363	0.713	0.404
2DS-III	2.883	1.244	0.349	0.277	0.839	0.405	0.794	0.450
4DS-I	2.898	1.251	0.349	0.277	0.844	0.407	0.798	0.452
$q^2 \in [9 - q_{max}^2] \text{ GeV}^2$								
SM	1.492	1.812	0.285	0.5	1.164	0.648	1.359	0.452
1DS-I	1.676	2.036	0.285	0.5	1.307	0.728	1.527	0.508
1DS-II	1.462	1.776	0.285	0.5	1.141	0.635	1.332	0.443
2DS-I	1.785	2.168	0.285	0.5	1.393	0.776	1.627	0.542
2DS-II	1.689	2.052	0.285	0.5	1.318	0.734	1.539	0.512
2DS-III	1.882	2.286	0.285	0.5	1.469	0.818	1.715	0.571
4DS-I	1.892	2.298	0.285	0.5	1.476	0.822	1.724	0.574

TABLE IV: Numerical predictions for $B_s \rightarrow D_s \tau \bar{\nu}_\tau$ observables in various q^2 bins.

Scenarios	$BR \times 10^3$	$R_{D_s^*}$	$A_{FB}^{D_s^*}$	$P_\tau^{D_s^*}$	$F_L^{D_s^*}$	$F_T^{D_s^*}$
$q^2 \in [3.2 - 5] \text{ GeV}^2$						
SM	0.334	0.043	0.062	0.164	0.596	0.404
1DS-I	0.375	0.048	0.62	0.164	0.596	0.404
1DS-II	0.339	0.044	0.066	0.165	0.601	0.399
2DS-I	0.386	0.05	0.440	0.163	0.591	0.408
2DS-II	0.378	0.049	0.062	0.164	0.596	0.404
2DS-III	0.399	0.051	0.127	0.162	0.589	0.411
4DS-I	0.404	0.052	0.219	0.162	0.590	0.410
$q^2 \in [5 - 7] \text{ GeV}^2$						
SM	1.275	0.319	-0.063	-0.077	0.497	0.502
1DS-I	1.432	0.358	-0.063	-0.077	0.497	0.502
1DS-II	1.296	0.324	-0.058	-0.077	0.502	0.497
2DS-I	1.475	0.369	0.398	-0.078	0.493	0.507
2DS-II	1.443	0.361	-0.063	-0.077	0.497	0.502
2DS-III	1.525	0.381	0.017	-0.079	0.490	0.510
4DS-I	1.543	0.386	0.129	-0.078	0.491	0.509
$q^2 \in [7 - 9] \text{ GeV}^2$						
SM	1.713	0.460	-0.132	-0.304	0.413	0.586
1DS-I	1.925	0.517	-0.132	-0.304	0.413	0.586
1DS-II	1.743	0.469	-0.127	-0.303	0.418	0.582
2DS-I	1.981	0.532	0.331	-0.304	0.409	0.591
2DS-II	1.940	0.521	-0.132	-0.304	0.413	0.586
2DS-III	2.047	0.550	-0.051	-0.304	0.406	0.594
4DS-I	2.071	0.557	0.061	-0.304	0.407	0.593
$q^2 \in [9 - q_{max}^2] \text{ GeV}^2$						
SM	0.984	0.536	-0.114	-0.463	0.359	0.641
1DS-I	1.105	0.602	-0.114	-0.463	0.359	0.641
1DS-II	1.002	0.546	-0.111	-0.463	0.363	0.637
2DS-I	1.136	0.619	0.212	-0.463	0.354	0.645
2DS-II	1.114	0.607	-0.114	-0.463	0.359	0.641
2DS-III	1.172	0.639	-0.057	-0.463	0.352	0.648
4DS-I	1.187	0.647	0.022	-0.463	0.353	0.647

TABLE V: Numerical predictions for $B_s \rightarrow D_s^* \tau \bar{\nu}_\tau$ observables in q^2 bins.

Scenarios	$\chi_1^{D_s^*}$	$\chi_2^{D_s^*}$	$\chi_3^{D_s^*}$	$\chi_4^{D_s^*}$	$\chi_5^{D_s^*}$	$\chi_6^{D_s^*}$
$q^2 \in [3.2 - 5] \text{ GeV}^2$						
SM	0.023	0.020	0.025	0.018	0.026	0.017
1DS-I	0.026	0.023	0.028	0.02	0.029	0.019
1DS-II	0.023	0.020	0.025	0.018	0.026	0.017
2DS-I	0.036	0.014	0.029	0.021	0.029	0.02
2DS-II	0.026	0.023	0.028	0.020	0.029	0.020
2DS-III	0.029	0.022	0.030	0.022	0.03	0.021
4DS-I	0.032	0.020	0.03	0.022	0.031	0.021
$q^2 \in [5 - 7] \text{ GeV}^2$						
SM	0.150	0.169	0.147	0.172	0.159	0.160
1DS-I	0.168	0.190	0.165	0.193	0.179	0.180
1DS-II	0.152	0.171	0.15	0.174	0.163	0.161
2DS-I	0.258	0.111	0.170	0.199	0.182	0.187
2DS-II	0.169	0.192	0.166	0.194	0.180	0.181
2DS-III	0.194	0.187	0.176	0.206	0.187	0.194
4DS-I	0.218	0.168	0.178	0.208	0.190	0.196
$q^2 \in [7 - 9] \text{ GeV}^2$						
SM	0.200	0.261	0.160	0.300	0.190	0.27
1DS-I	0.225	0.293	0.180	0.337	0.214	0.303
1DS-II	0.204	0.264	0.163	0.305	0.196	0.272
2DS-I	0.354	0.178	0.185	0.347	0.218	0.315
2DS-II	0.226	0.295	0.182	0.340	0.216	0.306
2DS-III	0.261	0.289	0.191	0.359	0.224	0.327
4DS-I	0.295	0.261	0.194	0.363	0.227	0.33
$q^2 \in [9 - q_{max}^2] \text{ GeV}^2$						
SM	0.237	0.299	0.144	0.392	0.192	0.344
1DS-I	0.267	0.335	0.162	0.441	0.216	0.386
1DS-II	0.243	0.303	0.147	0.40	0.198	0.348
2DS-I	0.375	0.244	0.166	0.453	0.219	0.399
2DS-II	0.269	0.338	0.163	0.444	0.218	0.389
2DS-III	0.301	0.338	0.172	0.467	0.225	0.414
4DS-I	0.330	0.316	0.174	0.473	0.228	0.418

TABLE VI: Numerical predictions for observables of $B_s \rightarrow D_s^* \tau \bar{\nu}_\tau$ in q^2 bins

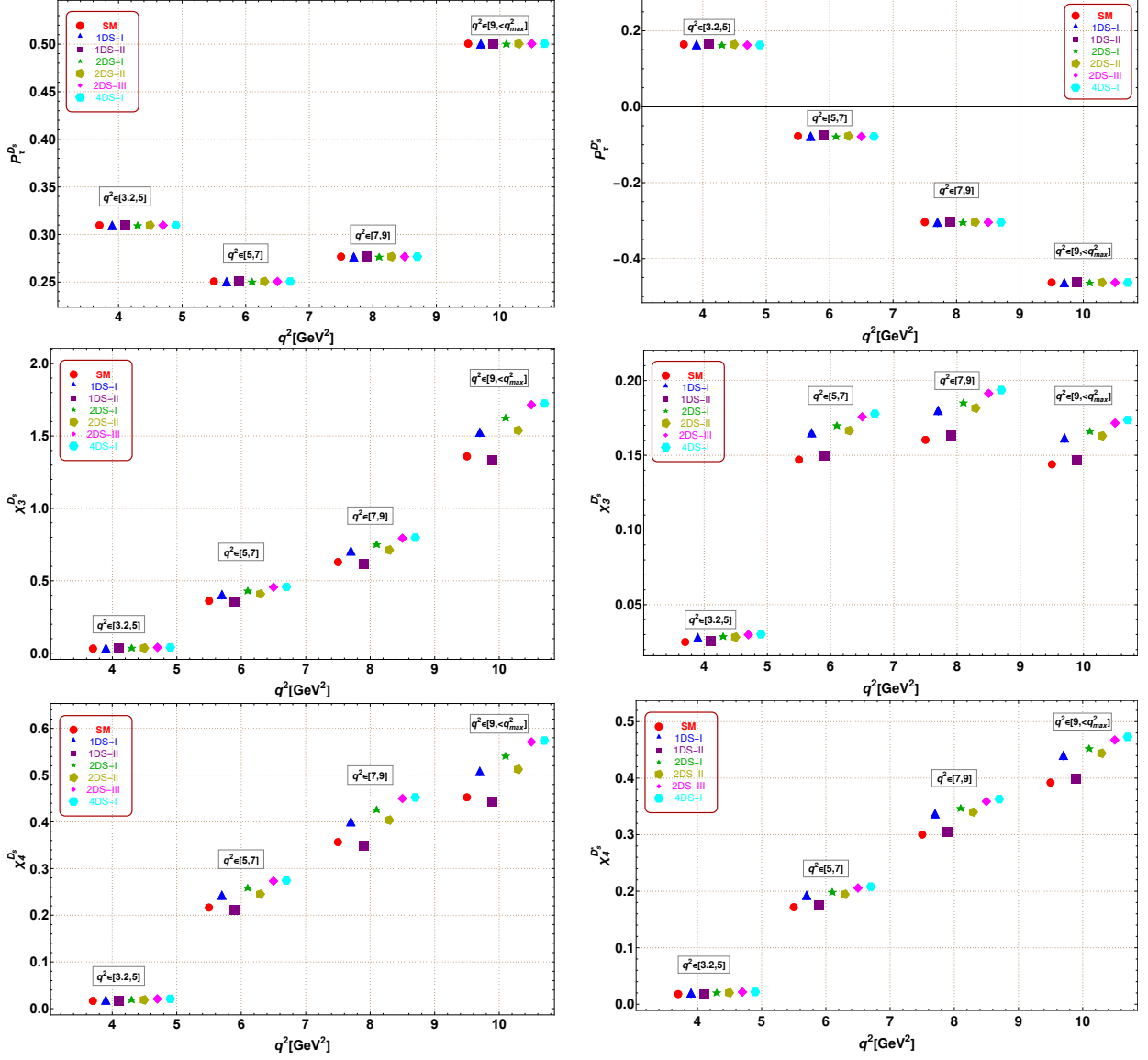


FIG. 6: Same as Fig. 3 for $P_\tau^{D_s}$ (top left panel), $P_\tau^{D_s^*}$ (top right panel), $\chi_3^{D_s}$ (middle left panel), $\chi_3^{D_s^*}$ (middle right panel), $\chi_4^{D_s}$ (bottom left panel) and $\chi_4^{D_s^*}$ (bottom right panel).

- **Branching Ratio:** Significant deviations from the SM predictions have been observed for the branching ratios of the decay processes $B_s \rightarrow D_s^{(*)}\tau\bar{\nu}_\tau$ in the q^2 bins [5, 7] and [7, 9], particularly for the 2DS-III and 4DS-I scenarios.
- **Lepton Non-universality:** The new physics contributions in the first q^2 bin show no effect. However, the 2DS-III and 4DS-I scenarios exhibit significant effects on the lepton non-universality (LNU) parameters in the other q^2 bins.
- **Forward Backward Asymmetry:** There is no deviation in the forward-backward

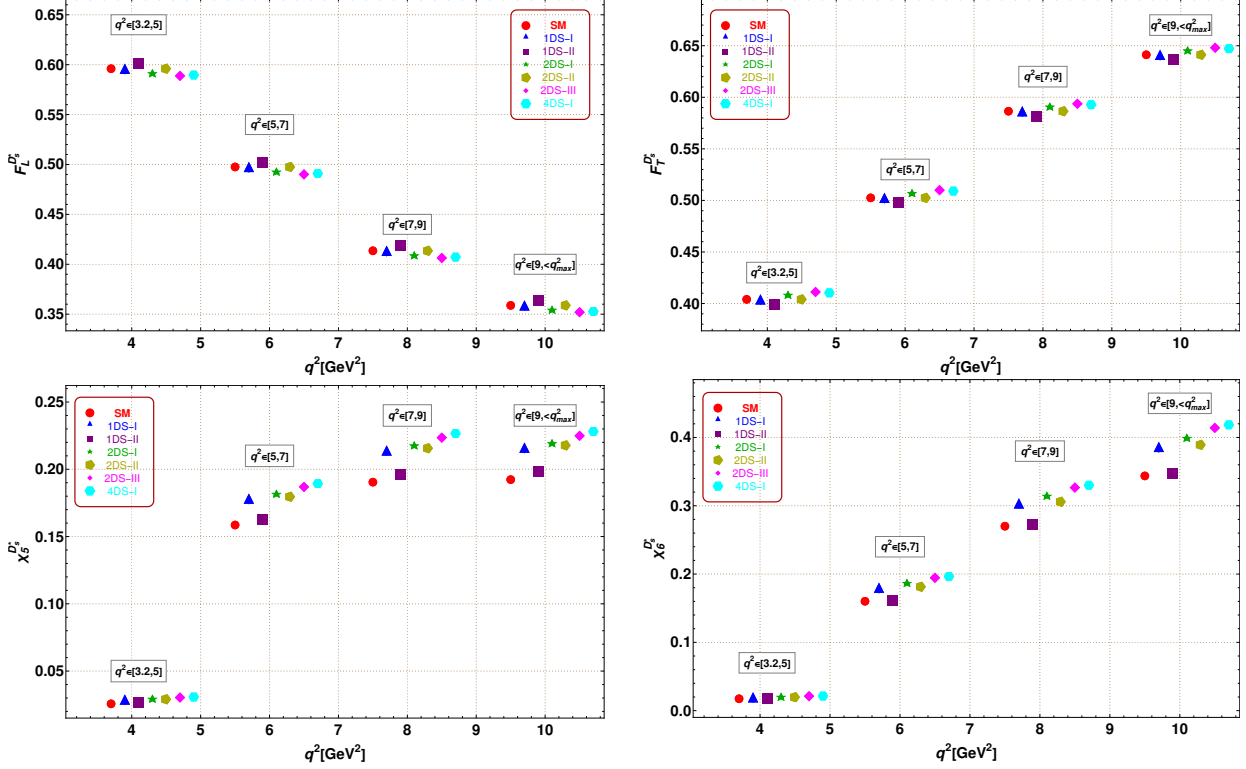


FIG. 7: Same as Fig. 3 for $F_L^{D_s^*}$ (top left panel), $F_T^{D_s^*}$ (top right panel), $\chi_5^{D_s^*}$ (bottom left panel) and $\chi_6^{D_s^*}$ (bottom right panel).

asymmetry of the decay modes $B_s \rightarrow D_s \tau \bar{\nu}_\tau$. In contrast, significant deviations are found for the decay process $B_s \rightarrow D_s^* \tau \bar{\nu}_\tau$ across all q^2 bins. The contributions from the 2DS-I scenario are the most pronounced, followed by the 4DS-I scenario. The forward-backward asymmetry is positive for both the 2DS-I and 4DS-I scenarios, and the zero-crossing of $A_{FB}^{D_s^*}$ is shifted to the third bin for the 2DS-III scenario.

- **τ Polarization Asymmetry:** No deviations have been found in the $P_\tau^{D_s^{(*)}}$ observables due to the presence of new physics scenarios.
- **D_s^* Polarization Asymmetry:** The contributions from the new physics coefficients to the longitudinal and transverse polarization asymmetries are very marginal.
- **Observables $\chi_{1,\dots,6}^{D_s^{(*)}}$:** The observables $\chi_{1,2}^{D_s}$ exhibit deviations due to the 2DS-III and 4DS-I scenarios. The observable $\chi_1^{D_s^*}$ shows significant effects from the 2DS-I, 4DS-I, and 1DS-I scenarios, while $\chi_2^{D_s^*}$ is notably affected by the 1DS-I, 2DS-II, and 4DS-I scenarios. The first bins of the observables $\chi_{3,4}^{D_s^{(*)}}$ show no deviations with the inclusion

of new physics. However, the fourth bin of $\chi_3^{D_s^*}$ receives significant contributions from the 4DS-I scenario. Except for 1DS-I, all other new physics scenarios exhibit substantial deviations from the SM in the second, third, and fourth q^2 bins of the $\chi_3^{D_s^*}$ observable. Additionally, the observables $\chi_4^{D_s^{(*)}}$ show deviations in the third and fourth bins due to the influence of new physics.

IV. CONCLUSION

In conclusion, we investigated the $b \rightarrow c\tau\bar{\nu}_\tau$ decays, specifically focusing on $B_s \rightarrow D_s^{(*)}\tau\bar{\nu}_\tau$, using a model-independent approach. We examined the sensitivity of the (axial)vector coefficients on branching ratios and various physical observables across four different q^2 bins: $q^2 \in [3.2, 5]$, $[5, 7]$, $[7, 9]$, and $[9, q_{\max}^2]$. The physical observables considered include forward-backward asymmetry, τ polarization asymmetry, D_s^* polarization asymmetry, lepton non-universality parameters, and the $\chi_{1,2,3,4,5,6}$ observables. We performed the analysis for six new physics scenarios, exploring all combinations of real and complex (axial)vector Wilson coefficients. Our findings indicate that the 2DS-III and 4DS-I scenarios significantly impact all observables across nearly all four q^2 bins, with some exceptions in the first bin for certain observables. However, the D_s^* and τ polarization asymmetries for the $B_s \rightarrow D_s^{(*)}\tau\bar{\nu}_\tau$ decay modes show no deviations from the SM predictions. Based on our analysis, we recommend investigating potential violations of lepton universality in the $B_s \rightarrow D_s^{(*)}\tau\bar{\nu}_\tau$ decay processes at B-factories and the LHCb experiment.

Acknowledgment

AKY acknowledges sincere thanks to the Government of India's DST-INSPIRE Fellowship division for their financial assistance (ID No. IF210687).

Appendix A: Helicity amplitudes for $B_s \rightarrow D_s^{(*)}\tau\bar{\nu}_\tau$

- $B_s \rightarrow D_s\tau\bar{\nu}_\tau$

The helicity amplitudes $H_{0,t}(q^2)$ of $B_s \rightarrow D_s$ decay mode in terms of the form factors

$f_{+,0}(q^2)$ are given as [33]

$$\begin{aligned} H_0(q^2) &= \sqrt{\frac{\lambda_{D_s}}{q^2}} f_+(q^2), \\ H_t(q^2) &= \frac{M_B^2 - M_{D_s}^2}{\sqrt{q^2}} f_0(q^2). \end{aligned} \quad (\text{A1})$$

- $B_s \rightarrow D_s^* \tau \bar{\nu}_\tau$

The helicity amplitudes $H_{V,\lambda}(q^2)$ ($\lambda = \pm, 0, t$) of $B_s \rightarrow D_s^*$ are given as [33]

$$\begin{aligned} H_{V,\pm}(q^2) &= (M_B + M_{D_s^*}) A_1(q^2) \mp \frac{\sqrt{\lambda_{D_s^*}}}{M_B + M_{D_s^*}} V(q^2), \\ H_{V,0}(q^2) &= \frac{M_B + M_{D_s^*}}{2 M_{D_s^*} \sqrt{q^2}} \left[- (M_B^2 - M_{D_s^*}^2 - q^2) A_1(q^2) + \frac{\lambda_{D_s^*}}{(M_B + M_{D_s^*})^2} A_2(q^2) \right], \\ H_{V,t}(q^2) &= - \frac{\sqrt{\lambda_{D_s^*}}}{\sqrt{q^2}} A_0(q^2). \end{aligned} \quad (\text{A2})$$

Appendix B: $B_s \rightarrow D_s$ form factors (Lattice QCD)

For the $B_s \rightarrow D_s$ decay, the form factors $f_{0,+}(q^2)$ with the Bourrely-Caprini-Lellouch (BCL) parameterization are defined as [37]

$$\begin{aligned} f_0(q^2) &= \frac{1}{\left(1 - \frac{q^2}{M_{B_c^0}^2}\right)} \sum_{n=0}^{N-1} a_n z^n(q^2), \\ f_+(q^2) &= \frac{1}{\left(1 - \frac{q^2}{M_{B_c^*}^2}\right)} \sum_{n=0}^{N-1} a_n \left(z^n(q^2) - \frac{n}{N} (-1)^{n-N} z^N(q^2) \right) \end{aligned} \quad (\text{B1})$$

where the z polynomial is expressed as

$$z(q^2) = \frac{\sqrt{t_+ - q^2} - \sqrt{t_+}}{\sqrt{t_+ - q^2} + \sqrt{t_+}},$$

Here, $t_+ = (M_{B_s} + M_{D_s})^2$, $N = 3$ and $M_{B_c^0} = 6.704$ and $M_{B_c^*} = 6.332$ are the physical pole mass [35]. Table VII includes the numerical values of the z -expansion coefficients in the full kinematic q^2 region, as calculated using the lattice QCD approach [35].

Form factor	z -Coefficients	Mean value
f_0	a_0	0.66574
	a_1	-0.25944
	a_2	-0.10636
f_+	a_0	0.66574
	a_1	-3.23599
	a_2	-0.07478

TABLE VII: Numerical value for z -coefficients for $B_s \rightarrow D_s$ decay in lattice QCD.

Appendix C: $B_s \rightarrow D_s^*$ form factors (Lattice QCD)

In Lattice QCD, the q^2 dependent form factors: $V(q^2)$ and $A_{0,1,2}(q^2)$, using the z -expansion are defined as [36, 38, 39]

$$F(q^2) = \frac{1}{P(q^2)} \sum_{n=0}^3 a_n z^n \mathcal{N}_n, \quad (\text{C1})$$

where

$$\begin{aligned} P(q^2) &= \prod_{M_{pole}} z(q^2, M_{pole}^2), \\ z(q^2, t_0) &= \frac{\sqrt{t_+ - q^2} - \sqrt{t_+ - t_0}}{\sqrt{t_+ - q^2} + \sqrt{t_+ - t_0}}, \end{aligned}$$

with

$$t_0 = (M_{B_s} - M_{D_s^*})^2, \quad t_+ = (M_B + M_{D^*})^2, \quad \mathcal{N}_n = 1.$$

Here, $P(q^2)$ is a pole function that includes poles resulting from $b\bar{c}$ where $A_0(q^2)$ is constructed with 0^- , $V(q^2)$ with 1^- and 1^+ states for $A_{1,2}(q^2)$. The predicted masses for the B_c pseudoscalar, vector, and axial vector states below the B_{D^*} threshold, which are incorporated into our pole factor, are presented in Table VIII. The z -expansion coefficient, a_n , is listed in Table IX.

[1] D. B. et al, Physics Letters B **395**, 373 (1997), ISSN 0370-2693, URL <https://www.sciencedirect.com/science/article/pii/S0370269397000713>.

$0^-/\text{GeV}$	$1^-/\text{GeV}$	$1^+/\text{GeV}$
6.275	6.335	6.745
6.872	6.926	6.75
7.25	7.02	7.15
7.28	7.15	

TABLE VIII: The physical masses of B_c pseudoscalar, axial vector and vector below the threshold BD^* .

	a_0	a_1	a_2	a_3
A_0	0.1047(57)	-0.43(13)	-0.10(96)	-0.03(1.00)
A_1	0.0552(21)	-0.010(54)	-0.03(77)	0.06(99)
A_2	0.059(11)	-0.11(22)	-0.25(79)	-0.05(1.00)
V	0.100(11)	-0.18(27)	-0.006(0.998)	0.0(1.0)

TABLE IX: The values of z -expansion coefficients (a_n) for the vector, axial-vector and pseudoscalar form factors for $B_s \rightarrow D_s^*$ decay.

- [2] J. E. Bartelt et al. (CLEO), Phys. Rev. Lett. **82**, 3746 (1999), hep-ex/9811042.
- [3] Y. S. Amhis et al. (HFLAV), Eur. Phys. J. C **81**, 226 (2021), 1909.12524.
- [4] F. U. Bernlochner, M. F. Sevilla, D. J. Robinson, and G. Wormser, Rev. Mod. Phys. **94**, 015003 (2022), 2101.08326.
- [5] M. Blanke, A. Crivellin, S. de Boer, T. Kitahara, M. Moscati, U. Nierste, and I. Nišandžić, Phys. Rev. D **99**, 075006 (2019), 1811.09603.
- [6] M. Fedele, M. Blanke, A. Crivellin, S. Iguro, T. Kitahara, U. Nierste, and R. Watanabe, Phys. Rev. D **107**, 055005 (2023), 2211.14172.
- [7] R. Dutta, A. Bhol, and A. K. Giri, Phys. Rev. D **88**, 114023 (2013), 1307.6653.
- [8] J. P. Lees et al. (BaBar), Phys. Rev. Lett. **109**, 101802 (2012), 1205.5442.
- [9] J. P. Lees et al. (BaBar), Phys. Rev. D **110**, 032018 (2024), 2311.15071.
- [10] M. Huschle et al. (Belle), Phys. Rev. D **92**, 072014 (2015), 1507.03233.
- [11] S. Hirose et al. (Belle), Phys. Rev. D **97**, 012004 (2018), 1709.00129.
- [12] G. Caria et al. (Belle), Phys. Rev. Lett. **124**, 161803 (2020), 1910.05864.

- [13] R. Aaij et al. (LHCb), Phys. Rev. Lett. **115**, 111803 (2015), [Erratum: Phys.Rev.Lett. 115, 159901 (2015)], 1506.08614.
- [14] R. Aaij et al. (LHCb), Phys. Rev. D **97**, 072013 (2018), 1711.02505.
- [15] H. Collaboration (HFLAV), “*preliminary average of $r(d)$ and $r(d^*)$ for summer 2023*” (2023), URL https://hflav-eos.web.cern.ch/hflav-eos/semi/summer23/html/RDsDsstar/RDRDs.html#:~:text=%200.284%20%C2%B1%200.012.%20*%200.357%20%C2%B1%200.029.
- [16] S. Fajfer, J. F. Kamenik, and I. Nisandzic, Phys. Rev. D **85**, 094025 (2012), 1203.2654.
- [17] J. A. Bailey et al. (MILC), Phys. Rev. D **92**, 034506 (2015), 1503.07237.
- [18] R. Aaij et al. (LHCb), Phys. Rev. Lett. **120**, 121801 (2018), 1711.05623.
- [19] J. Harrison, C. T. H. Davies, and A. Lytle (LATTICE-HPQCD), Phys. Rev. Lett. **125**, 222003 (2020), 2007.06956.
- [20] J. Koponen, Acta Phys. Polon. B **38**, 2893 (2007), hep-lat/0702006.
- [21] R.-H. Li, C.-D. Lu, and Y.-M. Wang, Phys. Rev. D **80**, 014005 (2009), 0905.3259.
- [22] A. Bhol, Europhysics Letters **106**, 31001 (2014), URL <https://dx.doi.org/10.1209/0295-5075/106/31001>.
- [23] M. Bordone, N. Gubernari, T. Huber, M. Jung, and D. van Dyk, Eur. Phys. J. C **80**, 951 (2020), 2007.10338.
- [24] R. Dutta and N. Rajeev, Phys. Rev. D **97**, 095045 (2018), 1803.03038.
- [25] S. Sahoo and R. Mohanta (2019), 1910.09269.
- [26] Y. Zhang, T. Zhong, H.-B. Fu, W. Cheng, L. Zeng, and X.-G. Wu, Phys. Rev. D **105**, 096013 (2022), 2202.02730.
- [27] S. Sahoo, R. Mohanta, and A. K. Giri, Springer Proc. Phys. **261**, 853 (2021).
- [28] B. Blossier, P.-H. Cahue, J. Heitger, S. La Cesa, J. Neuendorf, and S. Zafeiropoulos, Phys. Rev. D **105**, 054515 (2022), 2110.10061.
- [29] S. Sahoo and A. Bhol (2020), 2005.12630.
- [30] N. Gubernari, A. Khodjamirian, R. Mandal, and T. Mannel, JHEP **12**, 015 (2023), 2309.10165.
- [31] S. Rahmani and M. Ahwazian (2024), 2409.02460.
- [32] M. Tanaka and R. Watanabe, Phys. Rev. D **87**, 034028 (2013), 1212.1878.
- [33] Y. Sakaki, M. Tanaka, A. Tayduganov, and R. Watanabe, Phys. Rev. D **88**, 094012 (2013), 1309.0301.
- [34] S. Navas et al. (Particle Data Group), Phys. Rev. D **110**, 030001 (2024).

- [35] E. McLean, C. T. H. Davies, J. Koponen, and A. T. Lytle, Phys. Rev. D **101**, 074513 (2020), 1906.00701.
- [36] J. Harrison and C. T. H. Davies (HPQCD), Phys. Rev. D **105**, 094506 (2022), 2105.11433.
- [37] C. Bourrely, I. Caprini, and L. Lellouch, Phys. Rev. D **79**, 013008 (2009), [Erratum: Phys. Rev. D 82, 099902 (2010)], 0807.2722.
- [38] E. McLean, C. T. H. Davies, A. T. Lytle, and J. Koponen, Phys. Rev. D **99**, 114512 (2019), 1904.02046.
- [39] R. J. Hill, eConf **C060409**, 027 (2006), hep-ph/0606023.